Arabidopsis Leaf Flatness Is Regulated by PPD2 and NINJA through Repression of *CYCLIN D3* Genes[1][OPEN]

Alexandra Baekelandt,[a,b] Laurens Pauwels,[a,b] Zhibiao Wang,[c,d,2] Na Li,[c] Liesbeth De Milde,[a,b] Annelore Natran,[a,b] Mattias Vermeersch,[a,b] Yunhai Li,[c,d] Alain Goossens,[a,b] Dirk Inzé,[a,b,3,4,5] and Nathalie Gonzalez[a,b,3,5,6]

[a]Ghent University, Department of Plant Biotechnology and Bioinformatics, B-9052 Ghent, Belgium
[b]VIB Center for Plant Systems Biology, B-9052 Ghent, Belgium
[c]State Key Laboratory of Plant Cell and Chromosome Engineering, CAS Center for Excellence in Molecular Plant Sciences, Institute of Genetics and Developmental Biology, Chinese Academy of Sciences, Beijing 100101, China
[d]University of the Chinese Academy of Sciences, Beijing 100049, China

ORCID IDs: 0000-0003-0816-7115 (A.B.); 0000-0002-0221-9052 (L.P.); 0000-0001-5724-029X (L.D.M.); 0000-0002-1165-5622 (A.N.); 0000-0003-4173-2366 (M.V.); 0000-0002-0025-4444 (Y.L.); 0000-0002-1599-551X (A.G.); 0000-0002-3217-8407 (D.I.); 0000-0002-3946-1758 (N.G.)

In Arabidopsis (*Arabidopsis thaliana*), reduced expression of the transcriptional regulator *PEAPOD2* (*PPD2*) results in propeller-like rosettes with enlarged and dome-shaped leaves. However, the molecular and cellular processes underlying this peculiar phenotype remain elusive. Here, we studied the interaction between PPD2 and NOVEL INTERACTOR OF JAZ (NINJA) and demonstrated that *ninja* loss-of-function plants produce rosettes with dome-shaped leaves similar to those of *ppd* mutants but without the increase in size. We showed that *ninja* mutants have a convex-shaped primary cell cycle arrest front, putatively leading to excessive cell division in the central leaf blade region. Furthermore, *ppd* and *ninja* mutants have a similar increase in the expression of *CYCLIN D3;2* (*CYCD3;2*), and ectopic overexpression of *CYCD3;2* phenocopies the *ppd* and *ninja* rosette and leaf shape phenotypes without affecting the size. Our results reveal a pivotal contribution of NINJA in leaf development, in addition to its well-studied function in jasmonate signaling, and imply a new function for D3-type cyclins in, at least partially, uncoupling the size and shape phenotypes of *ppd* leaves.

Both between species and within the same organism, leaf morphology is diverse: leaves can be simple or compound, they can have margins that are smooth or serrated, and they can be flat or have various curvatures (Pérez-Pérez et al., 2002; Bilsborough et al., 2011; Dkhar and Pareek, 2014; Vlad et al., 2014). In Arabidopsis (*Arabidopsis thaliana*), leaf development starts with extensive cell proliferation throughout the leaf primordium. After a few days, cells at the tip of the leaf exit the mitotic cycle and a primary cell cycle arrest front moves in a tip-to-base direction, after which cells start to differentiate and expand (Donnelly et al., 1999; Kazama et al., 2010; Andriankaja et al., 2012). Simultaneously, meristemoid cells (i.e. small triangular cells that are dispersed throughout the leaf epidermis) can undergo up to three asymmetric divisions, allowing self-renewal and the formation of neighboring pavement cells (Bergmann and Sack, 2007; Pillitteri and Torii, 2012). Eventually, meristemoids differentiate into guard mother cells, which each divide symmetrically to produce the guard cells of a stomatal complex. Together with the primary arrest front, a secondary cell cycle arrest front that terminates the meristemoid cell divisions contributes to the total cell number and size of leaves (Geisler et al., 2000). Despite the knowledge of the cellular events determining leaf development, the molecular mechanisms governing the shape of growing tissues are still poorly understood. Genetic studies have identified a few genes that affect leaf flatness, such as the *CINCINNATA-like TEOSINTE BRANCHED1/CYCLOIDEA/PCF* (*TCP*) family involved in controlling the shape of the primary cell cycle arrest front (Nath et al., 2003; Efroni et al., 2008). Loss-of-function *tcp* mutants have a concave primary

[1]This work was supported by Ghent University (Bijzonder Onderzoeksfonds Methusalem project no. BOF08/01M00408). A.B. is an FWO predoctoral fellow (no. 131019) and L.P. an FWO postdoctoral fellow (no. 1206414N).

[2]Current address: School of Life Sciences, Beijing University of Chinese Medicine, Beijing 100029, China.

[3]These authors contributed equally to the article.

[4]Author for contact: dirk.inze@psb.vib-ugent.be.

[5]Senior author.

[6]Current address: Institut National de la Recherche Agronomique, Unité Mixte de Recherche 1332, Biologie du Fruit et Pathologie, CS20032, 33140 Villenave d'Ornon, France.

The author responsible for distribution of materials integral to the findings presented in this article in accordance with the policy described in the Instructions for Authors (www.plantphysiol.org) is: Dirk Inzé (dirk.inze@psb.vib-ugent.be).

A.B., L.P., and N.G. conceived the project and designed the experiments; A.B. performed most of the experiments and analyzed the data; N.L. and Z.W. performed the pull-down and bimolecular fluorescence complementation experiments; L.P. performed the yeast two-hybrid assay and L.D.M., A.N., and M.V. provided technical assistance; A.G., Y.L., D.I., and N.G. supervised the research; A.B. wrote the article; N.G. and D.I. complemented the writing, and the remaining authors provided critical input.

[OPEN]Articles can be viewed without a subscription.
www.plantphysiol.org/cgi/doi/10.1104/pp.18.00327

cell cycle arrest front, leading to excessive growth at the leaf margins compared with the central zone, resulting in enlarged and crinkly leaves. On the other hand, down-regulation of the *PEAPOD* genes (*PPD1* and *PPD2*) results in plants demonstrating a typical propeller-like rosette composed of enlarged but narrow dome-shaped leaves (White, 2006; Gonzalez et al., 2015). This leaf morphology is at least partially due to excessive meristemoid asymmetric divisions hypothesized to be combined with a restricted extension capacity of the margin cells (White, 2006; Gonzalez et al., 2015). In addition, although the position of the primary cell cycle arrest front is not affected in the Arabidopsis *ppd* deletion (Δ*ppd*) mutant (White, 2006), the shape of the front is proposed to be convex, leading to a prolonged period of cell proliferation in the central leaf blade region (Karidas et al., 2015). Consequently, whereas the TCP proteins are important for the regulation of the shape of the primary cell division arrest front (Nath et al., 2003; Palatnik et al., 2003), the PPD proteins are hypothesized to act on both the primary (Karidas et al., 2015) and the secondary (White, 2006; Gonzalez et al., 2015) mitotic arrest fronts. However, how the PPD proteins control these cellular processes and how this ultimately results in the leaf size and shape phenotypes observed in *ppd* mutants remain largely elusive.

Previous studies of the PPD signaling pathway have identified PPD2 direct target genes (Gonzalez et al., 2015), PPD2 protein partners (Pauwels et al., 2010; Gonzalez et al., 2015), and proteins that mark PPD2 or its interaction partners for degradation (Wang et al., 2016; Li et al., 2018). PPD2 binds to the promoters of two of the three D3-type cyclin genes, *CYCD3;2* and *CYCD3;3*, and represses their transcription (Gonzalez et al., 2015). CYCD3s are important for cell number determination in developing leaves (Dewitte et al., 2007), and meristemoid initiation and activity are reduced in the *cycd3;1 cycd3;2 cycd3;3* triple mutant compared with the wild type (Elsner et al., 2012; Lau et al., 2014). To control *CYCD3* gene expression, PPD2 acts in a complex with the transcriptional repressors KINASE-INDUCIBLE DOMAIN INTERACTING8 (KIX8) and KIX9, and reduced expression of *KIX8* and *KIX9* also leads to the formation of propeller-like rosettes with enlarged and dome-shaped leaves (Gonzalez et al., 2015). PPD2 is also proposed to interact with NOVEL INTERACTOR OF JAZ (NINJA; Pauwels et al., 2010; Gonzalez et al., 2015), a transcriptional repressor with a well-characterized function in the jasmonic acid (JA) signaling pathway (Pauwels et al., 2010; Acosta et al., 2013; Gasperini et al., 2015). *ninja* loss-of-function mutants show increased JA signaling and display shorter roots mimicking the JA-mediated growth inhibition, even in the absence of the hormone (Acosta et al., 2013; Gasperini et al., 2015). Although much is known of the role of NINJA in JA signaling in the root, it remains elusive if NINJA plays a role during leaf development or transcriptionally coregulates downstream targets of PPD2.

Here, we studied the PPD2-NINJA interaction in great detail and phenotypically and molecularly characterized *ninja* mutants. We found that NINJA, in addition to its known function in JA signaling and root development, has a key role in leaf development, likely due to the transcriptional regulation of *CYCD3* expression. With these findings, we further elucidate the importance of the PPD signaling pathway in controlling leaf growth.

RESULTS

NINJA Interacts with PPD2 in Vitro and in *Nicotiana benthamiana* Leaves

In previously performed tandem affinity purification experiments in Arabidopsis cell suspension culture, NINJA was identified as a putative PPD2 protein partner (Pauwels et al., 2010; Gonzalez et al., 2015). We further investigated this interaction with an in vitro pull-down experiment (Fig. 1A). The PPD2 and NINJA proteins were fused to a GST and a His tag, respectively, and the fusion products were expressed in bacteria. Pull down of the GST-PPD2 fusion protein using glutathione-Sepharose beads and subsequent immunoblotting using an anti-His antibody confirmed that NINJA also interacts with PPD2 in vitro (Fig. 1A). To confirm the PPD2-NINJA interaction in planta, a bimolecular fluorescence complementation assay was performed. Coexpression of *nYFP* (*N-terminal fragment of YELLOW FLUORESCENT PROTEIN*)-*NINJA* and *cYFP* (*C-terminal fragment of YFP*)-*PPD2* in *N. benthamiana* leaves resulted in a strong YFP signal in the nuclei of epidermal cells (Fig. 1B), confirming that PPD2 interacts with NINJA.

Deletion of the NINJA C Domain Abolishes the Interaction with PPD2, and *NINJA* Loss of Function Results in Plants with Dome-Shaped Leaves

NINJA is characterized by three conserved protein domains: the A domain harboring a TOPLESS (TPL)-binding ERF-ASSOCIATED AMPHIPHILIC REPRESSION motif instrumental for transcriptional repression, the B domain with unknown function, and the C domain that mediates interaction with the JASMONATE ZIM-DOMAIN (JAZ) proteins (Pauwels et al., 2010). Similar to the JAZ proteins, the PPD proteins belong to class II of the TIFY protein family. PPD proteins are characterized by a specific N-terminal PPD domain essential for the interaction with the KIX proteins (Gonzalez et al., 2015), a ZINC-FINGER EXPRESSED IN INFLORESCENCE MERISTEM (ZIM) domain containing a highly conserved TIFY (TIF[F/Y] XG) motif and known to mediate homodimerization and heterodimerization among TIFY proteins, and a divergent C-terminal Jas domain (Bai et al., 2011; Cuéllar Pérez et al., 2014). To map the protein domains that are essential for the interaction between PPD2 and

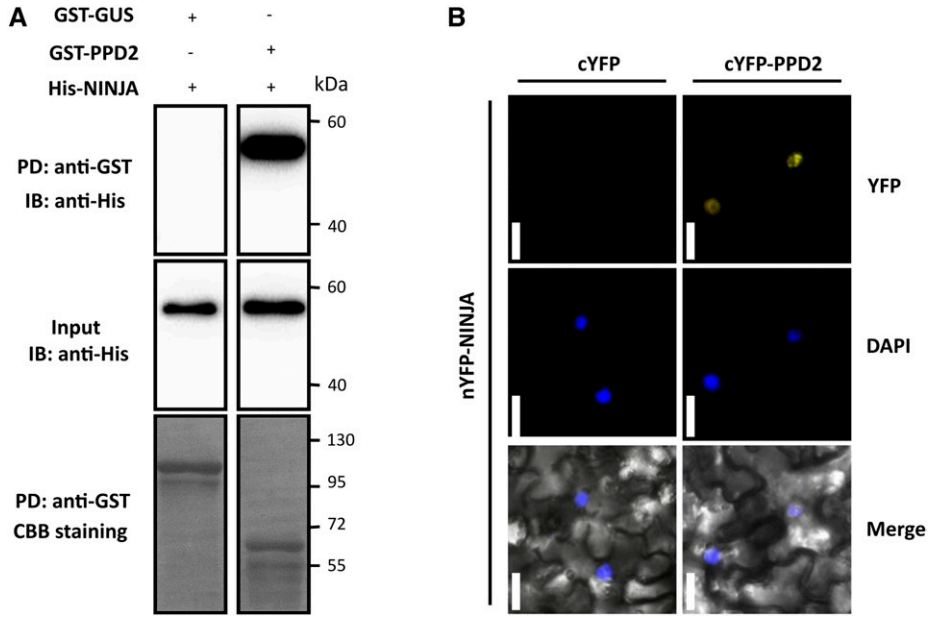

Figure 1. NINJA interacts with PPD2 in vitro and in *N. benthamiana* leaves. A, In a pull-down (PD) experiment, GST-PPD2 was immobilized on glutathione-Sepharose and the presence of His-NINJA was verified by immunoblotting (IB) using an anti-His antibody. GST-GUS was used as a negative control. The amount of GST-GUS or GST-PPD2 was visualized by Coomassie Brilliant Blue (CBB) staining. B, *nYFP-NINJA* and *cYFP-PPD2* or *cYFP* (as a negative control) were coexpressed in *N. benthamiana* leaves. 4′,6-Diamino-phenylindole (DAPI) staining indicates the nuclei. The DAPI-stained and bright-field microscopic images are merged in the bottom panels. Bars = 20 µm.

NINJA, we generated truncated versions of PPD2 that comprise different combinations of the three domains and tested these fragments for interaction with NINJA in a yeast two-hybrid (Y2H) assay. We found that the PPD2 ZIM domain is necessary and sufficient for the interaction with NINJA (Fig. 2A). A similar Y2H experiment using truncated versions of NINJA showed that PPD2 interacts with the C domain of NINJA (Fig. 2B). To uncover the potential involvement of NINJA in regulating leaf development, we phenotypically analyzed *ninja-1* and *ninja-2* mutants (Acosta et al., 2013; Gasperini et al., 2015). These mutants have a point mutation causing a premature stop codon in *NINJA* and, therefore, lack the C domain essential for interaction with PPD2 and show a significantly decreased expression of *NINJA* (Supplemental Fig. S1). When grown in soil for 25 d, *ninja* mutants produced propeller-like rosettes with narrow dome-shaped leaves (Fig. 2C) similar to those of *ppd2* (Fig. 2C; Wang et al., 2016) and *ami-ppd* (Gonzalez et al., 2015) plants. To investigate whether leaf size was changed in *ninja* mutants, the leaf areas of 25-d-old plants were measured, and the results are summarized in a heat map as the average percentage difference compared with the wild type (Fig. 2D). In the *ppd2* mutant, older leaves (L1–L6) were significantly larger and younger leaves (L9 onward) were significantly smaller than in the wild type. Although the younger leaves of *ninja* mutants were also significantly smaller (L6 onward), the older leaves had a similar size to those of the wild type (Fig. 2D).

In summary, we demonstrate that the C domain of NINJA interacts with the ZIM domain of PPD2 and that *ninja* loss-of-function mutants display a similar rosette and leaf curvature phenotype to *ppd2* plants, without an increased final leaf size.

The *ninja* Leaf Phenotype Is Not Influenced by Alterations in JA Response or Biosynthesis

Because NINJA is a negative regulator of JA signaling (Pauwels et al., 2010; Acosta et al., 2013; Gasperini et al., 2015), *ninja* mutants might lack the enlarged leaf size phenotype observed in *ppd2* mutants (Fig. 2D) as a result of an increased JA signaling pathway leading to growth inhibition (Acosta et al., 2013; Gasperini et al., 2015). To verify this, we used *ninja* plants crossed with the *allene oxide synthase* (*aos*) or *coronatine insensitive1* (*coi1-1*) mutant, in which the JA biosynthesis or response is abolished, respectively (Feys et al., 1994; Park et al., 2002; Thines et al., 2007; Pauwels et al., 2010). The *ninja-1 aos*, *ninja-2 aos*, and *ninja-1 coi1-1* double mutants were grown in soil for 25 d, and the size of the first four developing leaves (L1–L4) was measured. The leaf area of *ninja aos* (Fig. 3B) and *ninja-1 coi1-1* (Supplemental Fig. S2B) double mutants was not changed drastically compared with that of *ninja* or the wild type. In addition, the propeller-like rosette and dome-shaped phenotype of the *ninja aos* or *ninja-1 coi1-1* double mutant were indistinguishable from those of the

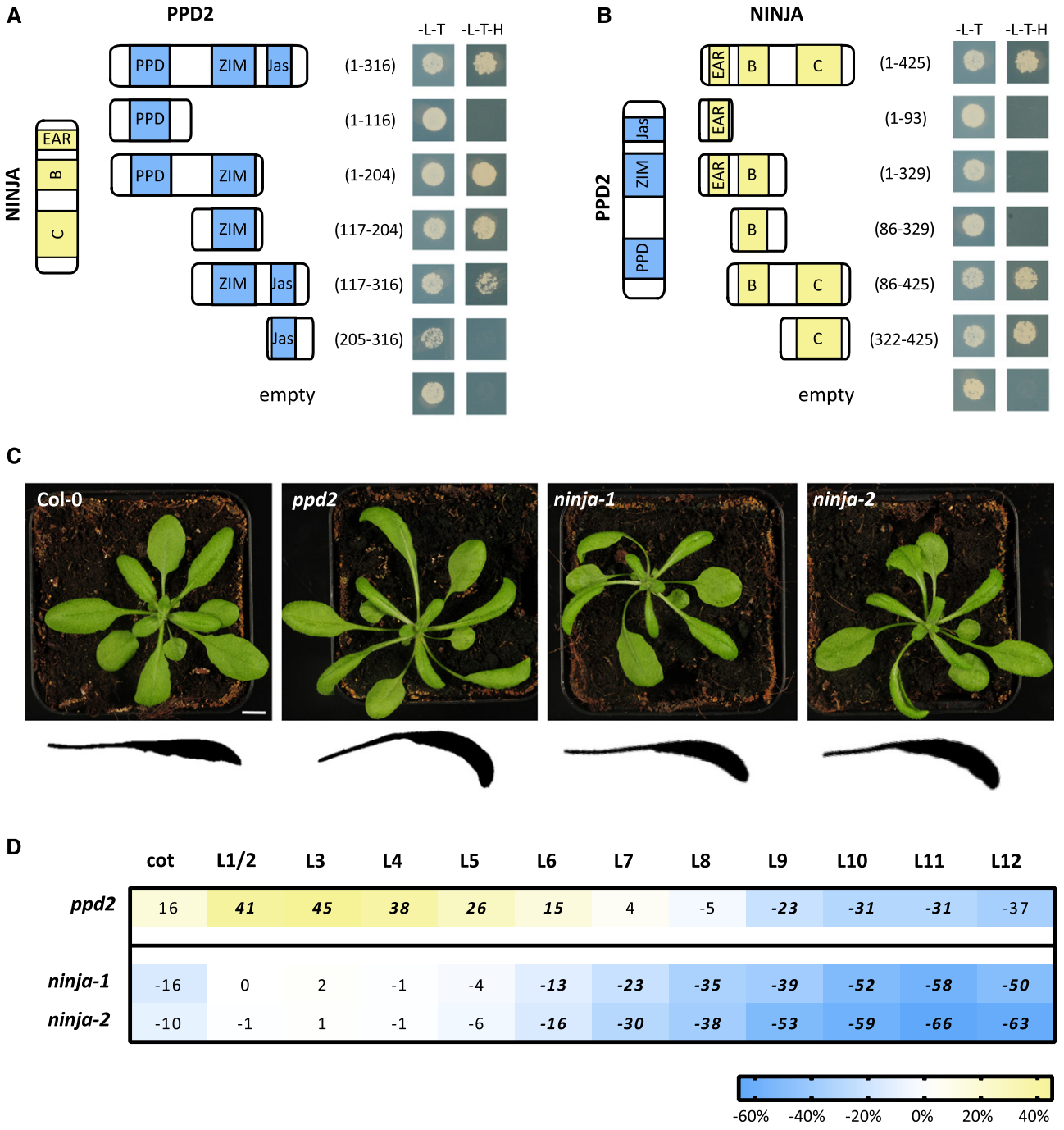

Figure 2. PPD2 interacts with the NINJA C domain. A and B, PPD2 (A) and NINJA (B) truncations were tested in Y2H assays to identify the specific domains for the PPD2-NINJA interaction. Transformants containing bait and prey constructs were grown on medium lacking Leu and Trp (-L-T) or Leu, Trp, and His (-L-T-H). Protein domains are represented, and numbers indicate terminal amino acid residues. C, Columbia-0 (Col-0), *ppd2*, *ninja-1*, and *ninja-2* plants grown in soil for 25 d. Side views of the seventh leaf (L7) are presented below the photographs. Bar = 1 cm. D, Area of the individual leaves of *ppd2* and *ninja* plants grown in soil for 25 d (n = 3 biological replicates with approximately eight plants per replicate), analyzed using mixed models in the SAS Enterprise Guide. Statistically significant differences ($P < 0.05$) relative to the wild type are marked in boldface italic type.

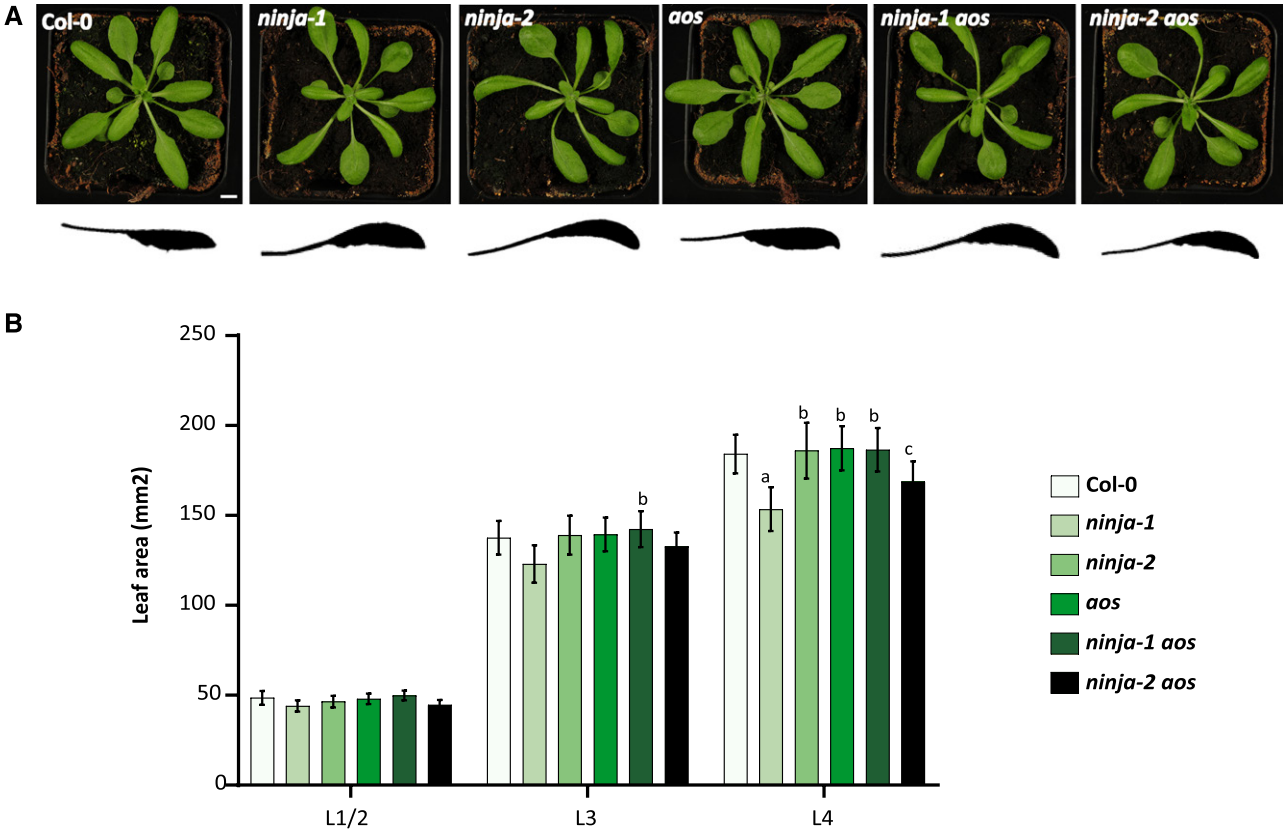

Figure 3. The *ninja* leaf phenotype is not affected by decreased JA biosynthesis. A, Col-0, *ninja-1*, *ninja-2*, *aos*, *ninja-1 aos*, and *ninja-2 aos* plants grown in soil for 25 d. Side views of the seventh leaf (L7) are presented below the photographs. Bar = 1 cm. B, Area of leaves 1/2, 3, and 4 of Col-0, *ninja-1*, *ninja-2*, *aos*, *ninja-1 aos*, and *ninja-2 aos* plants grown in soil for 25 d ($n = 3$ biological replicates with approximately eight plants per replicate). Error bars represent SE. Statistical significance was evaluated by ANOVA followed by Tukey's posthoc analysis. Significant differences ($P < 0.05$) relative to Col-0 (a), *ninja-1* (b), and *aos* (c) are indicated with lowercase letters.

ninja plants (Fig. 3A; Supplemental Fig. S2A; Gasperini et al., 2015).

In conclusion, we demonstrate that the propeller-like rosette and the not-enlarged and dome-shaped leaf phenotypes of *ninja* plants are not affected by a decreased JA response or biosynthesis.

ninja Leaves Have a Convex Primary Cell Cycle Arrest Front

In the Arabidopsis Landsberg *erecta* Δ*ppd* mutant, the shape of the primary cell cycle arrest front is hypothesized to be convex rather than straight, leading to excessive growth in the central region of the leaf contributing to the Δ*ppd* dome-shaped leaf phenotype (Karidas et al., 2015). Because PPD2 interacts with NINJA and *ninja* mutants also have a dome-shaped leaf phenotype, the underlying mechanism might be similar. To investigate alterations in the shape of the primary cell cycle arrest front in *ami-ppd* and *ninja-2* mutants, we made use of the *pCYCB1;1-DB*::*GUS* reporter line, a marker for actively dividing cells (Andriankaja et al., 2012). *pCYCB1;1-DB*::*GUS* and homozygous *ninja-2 pCYCB1;1-DB*::*GUS* and *ami-ppd pCYCB1;1-DB*::*GUS* double transgenic plants were grown in soil for 21 d, and young developing leaves of similar size were used for GUS staining. The shape of the primary arrest front appeared to be more convex in *ami-ppd pCYCB1;1-DB*::*GUS* and *ninja-2 pCYCB1;1-DB*::*GUS* leaves compared with the *pCYCB1;1-DB*::*GUS* control (Fig. 4A). The extent of convexity was quantified by measuring the perpendicular distance between the highest point of GUS signal in the center of the leaf and a horizontal line connecting the GUS signal at the leaf margins. We found that the distance between the position of the cell cycle arrest front in the central part of the leaf compared with the margins was increased significantly by 32% in *ami-ppd pCYCB1;1-DB*::*GUS* and 125% in *ninja-2 pCYCB1;1-DB*::*GUS* compared with the *pCYCB1;1-DB*::*GUS* control (Fig. 4B).

To summarize, the *ninja-2* mutant presents a convex primary cell cycle arrest front, as also observed in *ami-ppd* plants.

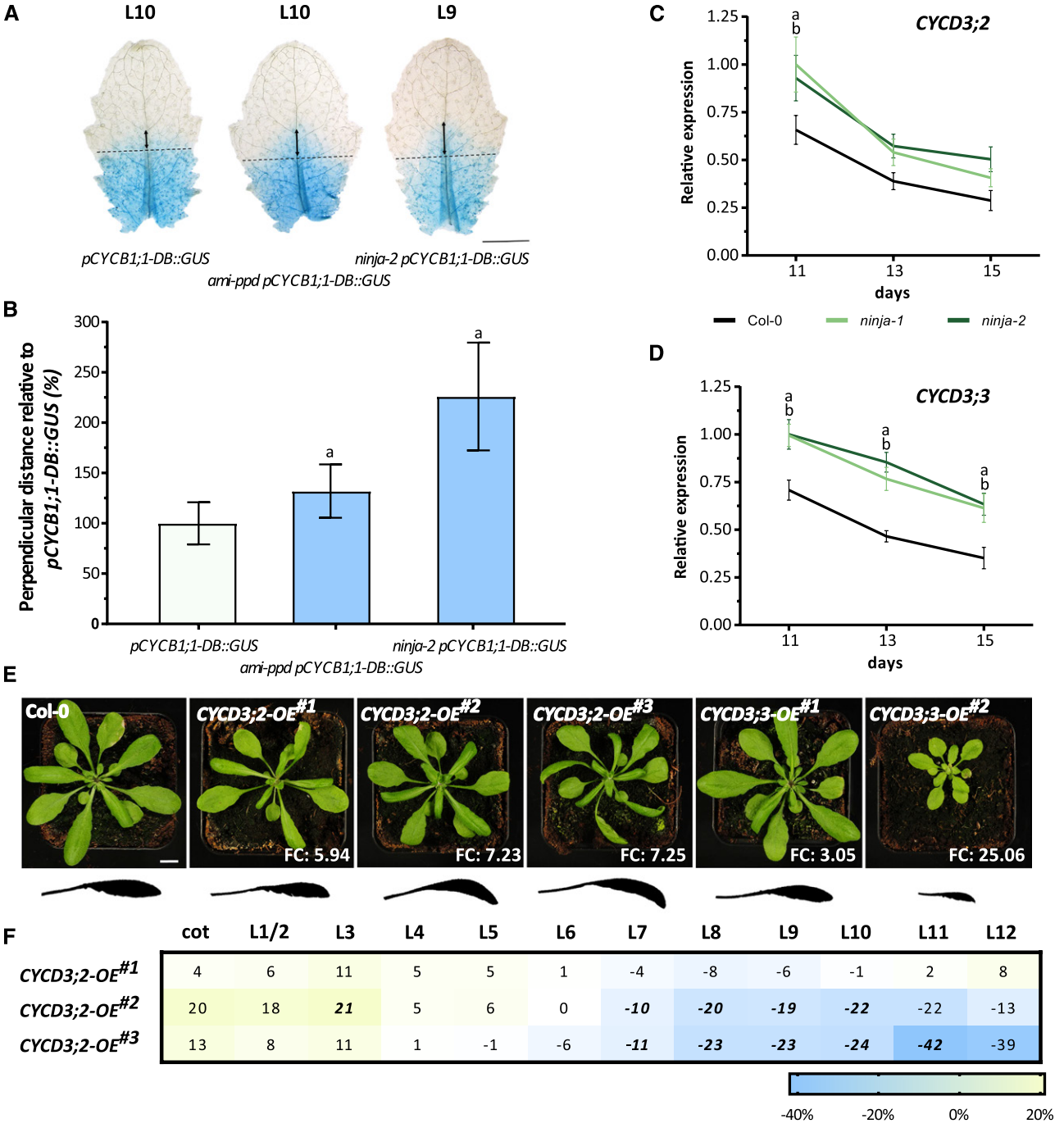

Figure 4. The *ninja* mutants have an increased expression of *CYCD3;2* and *CYCD3;3*, and *CYCD3;2-OE* plants have dome-shaped leaves. A and B, The primary cell cycle arrest front and the perpendicular distance between the highest point of the GUS signal in the center of the leaf and a horizontal line connecting the GUS signal at the leaf margins of leaf 9 or 10 of 21-d-old soil-grown Col-0, *ami-ppd*, and *ninja-2* plants expressing the *pCYCB1;1-DB*::*GUS* construct (n = 3 biological replicates with ~20 leaves per replicate). Error bars represent SE. Statistical significance was evaluated by ANOVA followed by Tukey's posthoc analysis. Significant differences ($P < 0.05$) relative to *pCYCB1;1-DB*::*GUS* are indicated with lowercase letter a. C and D, Col-0, *ninja-1*, and *ninja-2* plants were grown in vitro, and the first leaf pair (L1/2) was harvested after 11, 13, and 15 d for RNA extraction and qRT-PCR analysis to verify the expression of *CYCD3;2* and *CYCD3;3* (n = 3 biological replicates with approximately five leaves per replicate). Error bars represent SE. Statistical significance was evaluated by ANOVA followed by Tukey's posthoc analysis. Significant differences ($P < 0.05$) between Col-0 and *ninja-1* (a) or *ninja-2* (b) are indicated with lowercase letters. E, Col-0, *CYCD3;2-OE*$^{\#1\text{-}\#3}$, and *CYCD3;3-OE*$^{\#1\text{-}\#2}$ plants grown in soil for 25 d. Fold change (FC) values of transgene expression compared with the wild type are also provided. Side views of the seventh leaf (L7) are presented below the photographs. Bar = 1 cm. F, Area of individual leaves of *CYCD3;2-OE* plants grown in soil for 25 d (n = 3 biological replicates with

High Ectopic Expression of *CYCD3;2* Results in Plants with Dome-Shaped Leaves

Previously, we have shown that the expression of the cell cycle-related genes *CYCD3;2* and *CYCD3;3* is up-regulated in the *ami-ppd* mutant (Gonzalez et al., 2015). To verify if the expression of these cell cycle genes is also changed in the *ninja* mutants, *ninja-1* and *ninja-2* plants were grown in vitro and the first leaf pair (L1/2) was harvested after 11, 13, and 15 d for quantitative real time (qRT)-PCR analysis. For all time points, we observed increased expression of *CYCD3;2* and *CYCD3;3* in *ninja* plants compared with the wild type (Fig. 4, C and D), although for *CYCD3;2*, the difference in expression was only statistically significant at day 11 (Fig. 4C).

To study the potential involvement of CYCD3;2 and CYCD3;3 to control leaf flatness, we generated independent homozygous *CYCD3;2* and *CYCD3;3* overexpression (OE) lines in which the expression of the transgene was driven by the constitutive cauliflower mosaic virus *35S* promoter. For *CYCD3;2*, we obtained only lines with a relatively low transgene overexpression level compared with the wild type (fold change, 5.94–7.25; Fig. 4E). Interestingly, the lines with the highest transgene overexpression ($^{\#2}$ and $^{\#3}$; Fig. 4E) produced propeller-like rosettes with narrow dome-shaped leaves, whereas the leaf shape phenotype was less pronounced in the line with a relatively lower *CYCD3;2* overexpression level ($^{\#1}$; Fig. 4E). Upon *CYCD3;3* overexpression, plants did not show an effect on leaf curvature, but growth was reduced in the transgenic line with the highest level of overexpression ($^{\#2}$; Fig. 4E).

To study leaf size in the *CYCD3;2-OE* lines, individual leaf areas of 25-d-old, soil-grown plants were measured, and the results are summarized in a heat map as the average percentage difference compared with the wild type (Fig. 4F). Although the *CYCD3;2-OE*$^{\#1}$ mutant did not show alterations in leaf size, the *CYCD3;2-OE*$^{\#2\text{-}\#3}$ mutants had significantly decreased areas of the younger leaves (L7 onward), whereas the area of the older leaves was not changed significantly (Fig. 4F).

In summary, we demonstrate that the expression of *CYCD3;2* and *CYCD3;3* was increased in *ninja* plants and that transgenic lines overexpressing *CYCD3;2* produced propeller-like rosettes with dome-shaped leaves. In the *CYCD3;2-OE* line with the lowest overexpression level, the rosette and leaf shape phenotype of *ppd* and *ninja* mutants was only poorly recapitulated, whereas the increase in *CYCD3;2* expression was more pronounced than in the *ninja* mutants. We hypothesize that the expression of *CYCD3;2* in *ppd* and *ninja* mutants may be extremely high in specific cells but cannot be identified as such because entire leaves were harvested for the expression analysis. Despite the leaf curvature phenotype, the leaf areas of *CYCD3;2-OE* plants were not increased compared with those of the wild type, which is in contrast to the leaf size phenotype of *ppd* mutants but in line with that of *ninja* plants.

CYCD3;2-OE Plants Have an Increased Number of Pavement Cells, But Their Meristemoid Asymmetric Division Is Not Changed Drastically

ppd loss-of-function mutants have an increased number of pavement and guard cells (White, 2006; Gonzalez et al., 2015). In addition, asymmetric divisions of meristemoids are increased in the *ami-ppd* mutant compared with the wild type (Gonzalez et al., 2015). If *CYCD3;2* is the downstream target gene of the PPD2 signaling pathway responsible for the dome-shaped leaf phenotype, we hypothesize that similar cellular alterations might be present in *CYCD3;2-OE* plants compared with *ppd* loss-of-function mutants. To verify this, *CYCD3;2-OE* plants with a visibly mild ($^{\#1}$) and a strong ($^{\#2}$) leaf curvature phenotype were grown in soil for 25 d, and a cellular analysis of the lower (abaxial) epidermis of L1/2 was performed (Fig. 5). Whereas the area of L1/2 in the *CYCD3;2-OE* lines was not changed significantly compared with the wild type (Fig. 4F), they showed increased numbers of guard cells ($^{\#1}$ 10%, $^{\#2}$ 22%), pavement cells ($^{\#1}$ 20%, $^{\#2}$ 60%), and, consequently, total epidermal cells ($^{\#1}$ 17%, $^{\#2}$ 46%; Fig. 5A). Accordingly, the average pavement cell area was lower than that of the wild type ($^{\#1}$ –10%, $^{\#2}$ –25%; Fig. 5A). A cell size distribution analysis, in which cells are categorized based on their size and the relative frequency of cells within each category is determined, showed that the abaxial epidermis of the *CYCD3;2-OE* lines contained more small cells (less than 8,000 μm^2), whereas cells with a minimal area of greater than 8,000 μm^2 were less abundant than in the wild type (Fig. 5B). The stomatal index (i.e. the number of stomata per total epidermal cell number) was decreased in the *CYCD3;2-OE* lines ($^{\#1}$ –6%, $^{\#2}$ –16%; Fig. 5A). Because the decreased stomatal index and increased relative frequency of small cells in *CYCD3;2-OE* leaves might result from increased meristemoid asymmetric divisions, individual meristemoids in L1/2 of *CYCD3;2-OE*$^{\#2}$ plants were followed for three successive days (D12–D14) using leaf imprints, and the number of asymmetric divisions (Fig. 5C, top), guard mother cells, and stomata formation events were scored. In contrast to the increased meristemoid asymmetric division observed in the *ami-ppd* mutant compared with the wild type (Gonzalez et al., 2015), we did not detect increased meristemoid asymmetric divisions in the *CYCD3;2-OE*$^{\#2}$ plants (D12 and D13, $^{\#2}$ 24% versus $^{\text{Col-0}}$ 42%; Fig. 5C, middle). Also, among meristemoids that divided asymmetrically, the

Figure 4. (*Continued*.)
approximately eight plants per replicate), analyzed using mixed models in the SAS Enterprise Guide. Statistically significant differences ($P < 0.05$) relative to the wild type are marked in boldface italic type.

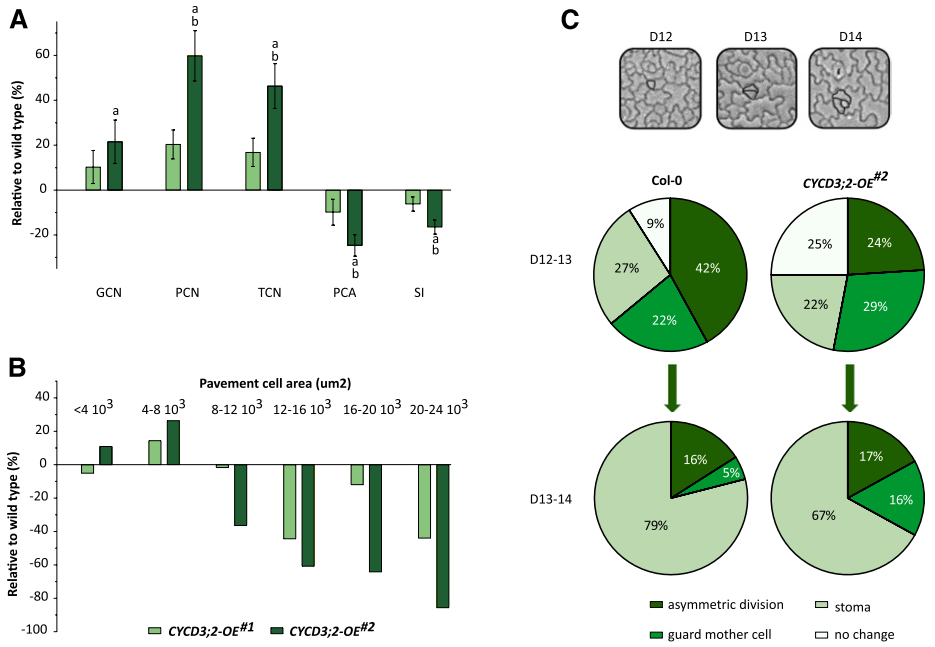

Figure 5. *CYCD3;2-OE* leaves have a higher frequency of small cells but their meristemoid asymmetric divisions are not changed drastically. A, Average guard cell number (GCN), pavement cell number (PCN), total cell number (TCN), pavement cell area (PCA), and stomatal index (SI) in the lower (abaxial) epidermis of the first leaf pair (L1/2) of *CYCD3;2-OE*$^{\#1}$ and *CYCD3;2-OE*$^{\#2}$ mutants relative to Col-0 (n = 3 biological replicates with four leaves per replicate). Error bars represent SE. Statistical significance was evaluated by ANOVA followed by Tukey's posthoc analysis. Significant differences ($P < 0.05$) relative to Col-0 (a) and *CYCD3;2-OE*$^{\#1}$ (b) are indicated with lowercase letters. B, For the pavement cell size distribution, cells are divided into bins of 4,000 μm^2 according to their area. C, Individual meristemoids in the abaxial epidermis of L1/2 of Col-0 and *CYCD3;2-OE*$^{\#2}$ mutants were followed for three successive days (D12–D14), and asymmetric division, guard mother cell, and stoma formation events were scored. Arrows, To score the recurrent asymmetric events, only meristemoids that divided asymmetrically in the D12-D13 transition were taken into account.

rate of recurrent asymmetric division on the following day was similar in *CYCD3;2-OE*$^{\#2}$ and wild-type plants (D13 and D14, $^{\#2}$ 17% versus $^{\text{Col-0}}$ 16%; Fig. 5C, bottom).

In conclusion, *CYCD3;2-OE* leaves show increased guard and pavement cell numbers and decreased average pavement cell areas. Despite the decrease in stomatal index, meristemoid asymmetric divisions were similar, or even decreased slightly, in *CYCD3;2-OE* compared with the wild type.

ppd2, *ninja*, and *CYCD3;2-OE* Plants Have Dome-Shaped Leaves, Albeit To a Different Extent

To compare the leaf curvature of *ppd2*, *ninja-1*, and *CYCD3;2-OE* plants, they were grown in soil for 25 d, the seventh leaf (L7) was harvested, and the leaf area, length, width, and perimeter were measured before (projected) and after (real) leaves were cut to flatten them (Fig. 6A; Supplemental Fig. S3). The width and perimeter of the leaf lamina were reduced in PPD2 signaling mutants compared with the wild type (width, $^{\#1}$ –6%, $^{\#2}$ –6%, $^{ninja\text{-}1}$ –19%, ^{ppd2} –14%; perimeter, $^{\#1}$ –5%, $^{\#2}$ –4%, $^{ninja\text{-}1}$ –10%, ^{ppd2} –16%), being statistically significant for *ninja-1* and *ppd2* leaves, whereas the leaf length did not differ between mutants and the wild type (Supplemental Fig. S3). As a read out for the narrowness of the leaves, the length-to-width ratio was calculated, and as a proxy for the extent of leaf curvature, we calculated the percentage difference between the projected and real leaf area, length, and width. For all mutant lines, the leaf length-to-width ratio was significantly greater than for the wild type ($^{\#1}$ 8%, $^{\#2}$ 12%, $^{ninja\text{-}1}$ 27%, ^{ppd2} 16%; Fig. 6B), indicating that the leaves were narrower and more elliptic. The decreases in projected-to-real leaf area, length, and width (Fig. 6C) were significantly more pronounced in *ppd2* (area, –47%; length, –20%; width, –44%) and *ninja-1* (area, –41%; length, –12%; width, –41%) mutants compared with the wild type (area, –28%; length, –7%; width, –30%). A similar trend was observed in the *CYCD3;2-OE*$^{\#2}$ mutant (area, –33%; length, –6%; width, –39%), although it was significant only for the projected-to-real leaf area and width differences (Fig. 6C). Despite the parallel alterations in the leaf length, width, perimeter, length-to-width ratio, and projected-to-real leaf area, length, and width differences compared with the wild type, all findings were least pronounced in the *CYCD3;2-OE* lines and most pronounced in the *ppd2* mutant.

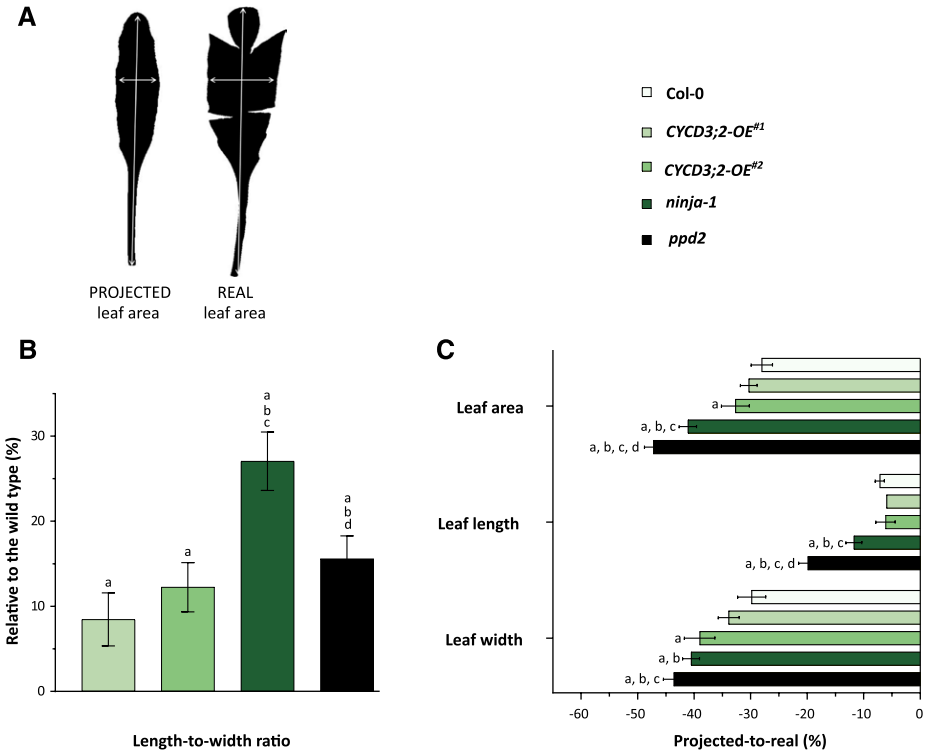

Figure 6. PPD2 signaling mutants have narrow and dome-shaped leaves. A, The leaf area, length, and width were measured before (projected) and after (real) leaf 7 (L7) was cut to flatten. B and C, Leaf 7 length-to-width ratio (B) and projected-to-real leaf area, length, and width (C) of Col-0, *CYCD3;2-OE*$^{\#1}$, *CYCD3;2-OE*$^{\#2}$, *ninja-1*, and *ppd2* plants grown in soil for 25 d ($n = 3$ biological replicates with approximately eight plants per replicate). Error bars represent SE. Statistical significance was evaluated by ANOVA followed by Tukey's posthoc analysis. Significant differences ($P < 0.05$) relative to Col-0 (a), *CYCD3;2-OE*$^{\#1}$ (b), *CYCD3;2-OE*$^{\#2}$ (c), and *ninja-1* (d) are indicated with lowercase letters.

To summarize, *ppd2*, *ninja-1*, and *CYCD3;2-OE* plants have an increased leaf length-to-width ratio, reflecting the narrower leaves and decreased projected-to-real leaf area, length, and width compared with the wild type, which represents the dome-shaped phenotype.

Inactivation of CYCD3;1 and CYCD3;2 Partially Restores the *ppd* Leaf Phenotype

The leaf curvature and cellular phenotype in *CYCD3;2-OE* lines together with the increased expression of *CYCD3;2* in *ami-ppd* (Gonzalez et al., 2015) and *ninja* plants suggest that elevated levels of *CYCD3;2* cause the dome-shaped leaf phenotype in these mutants. To test this hypothesis, homozygous *ppd2 cycd3;2* double mutants were generated and grown in soil with the corresponding single mutants to measure the areas of L1 to L4 and the curvature of L7 after 25 d (Supplemental Fig. S4). At the rosette level, the *ppd2 cycd3;2* double mutant showed a clear propeller-like phenotype (Supplemental Fig. S4A). In addition, the narrow and dome-shaped leaf phenotype was not reversed in *ppd2 cycd3;2* compared with *ppd2*, which was reflected by a similar length-to-width ratio and projected-to-real leaf area, length, and width (Supplemental Fig. S4, B and C). Finally, the *ppd2* leaf size increase (Wang et al., 2016) was retained in *ppd2 cycd3;2* plants (Supplemental Fig. S4D). Arabidopsis has three D3-type cyclins, which were considered previously to act redundantly (Dewitte et al., 2007). In contrast to *CYCD3;2-OE* plants, *CYCD3;3-OE* plants did not display curved leaves (Fig. 4E). On the other hand, constitutive overexpression of *CYCD3;1* has been shown to lead to dramatic changes in Arabidopsis leaf morphology, including extensive curling and an increased number of small cells (Riou-Khamlichi et al., 1999; Dewitte et al., 2003). Although the expression of *CYCD3;1* was not changed in L1/2 of 13-d-old *ami-ppd* plants (Gonzalez et al., 2015) and in L1/2 of 11-, 13-, and 15-d-old *ninja* mutants (Supplemental Fig. S5), *CYCD3;1* was identified previously as a putative target of PPD2 (Gonzalez et al., 2015). Therefore, we transformed the *cycd3;1 cycd3;2* double mutant with the *ami-ppd* construct (Gonzalez et al., 2015). We quantified the expression of *PPD2* in L1/2 of 14-d-old in vitro-grown plants to ensure that the construct had a similar functionality in the *cycd3;1 cycd3;2* double mutant to that in a wild-type background, and two independent single-locus insertion *cycd3;1 cycd3;2 ami-ppd* mutants ($^{\#1\text{-}\#2}$) with a *PPD2* down-regulation similar to that of the *ami-ppd* line were selected (Supplemental

Fig. S6). Of these lines, the area of L1 to L4 and the curvature of L7 were measured and compared with those of the wild type, the *ami-ppd* line, and the *cycd3;1 cycd3;2* double mutant. The propeller-like appearance of the rosette (Fig. 7A) and the narrow-leaf phenotype, reflected by the length-to-width ratio (Fig. 7B), were less pronounced in the *cycd3;1 cycd3;2 ami-ppd* mutants compared with the *ami-ppd* mutant ($^{\#1}$ 11%, $^{\#2}$ 13% versus $^{ami\text{-}ppd}$ 18%), although not completely restored to those of the wild type. The projected-to-real leaf area ($^{\#1}$ −29%, $^{\#2}$ −25% versus $^{ami\text{-}ppd}$ −47%), length ($^{\#1}$ −12%, $^{\#2}$ −14% versus $^{ami\text{-}ppd}$ −22%), and width ($^{\#1}$ −25%, $^{\#2}$ −26% versus $^{ami\text{-}ppd}$ −43%) differences were significantly higher in the *cycd3;1 cycd3;2 ami-ppd* mutants compared with the *ami-ppd* mutant (Fig. 7C), yet they were still reduced compared with the *cycd3;1 cycd3;2* plants (area, −10%; length, −6%; width, −7%). Interestingly, although the areas of L1 to L4 were reduced in *cycd3;1 cycd3;2 ami-ppd* compared with *ami-ppd* (Fig. 7D), they were still increased significantly compared with those of the wild type.

In conclusion, Arabidopsis CYCD3 proteins play a crucial role in limiting the leaf curvature observed in *ppd* loss-of-function mutants.

DISCUSSION

The Primary Cell Cycle Arrest Front Is Convex in *ninja* and *ppd* Mutants

NINJA is a transcriptional repressor with a pivotal role in JA signaling (Pauwels et al., 2010; Acosta et al., 2013; Gasperini et al., 2015). In the absence of JA, NINJA forms a complex with JAZ, MYC2, and TPL to prevent the expression of downstream JA-responsive genes (Thines et al., 2007; Pauwels et al., 2010; Bai et al., 2011; Li et al., 2017). Upon JA perception by the SCF^{COI1} ubiquitin ligase complex, JAZ proteins are degraded, the MYC2 transcription factor is released, and the expression of early JA-responsive genes is induced (Thines et al., 2007; Pauwels et al., 2010). Although the role of NINJA with regard to JA signaling has been studied intensively in both Arabidopsis and cotton (*Gossypium hirsutum*; Acosta et al., 2013; Gasperini et al., 2015; Wang et al., 2017), JA-independent roles of NINJA are largely unknown. NINJA has been identified as a putative interaction partner of PPD2 in a tandem affinity purification experiment performed in an Arabidopsis cell suspension culture (Gonzalez et al., 2015). In this study, we confirmed this interaction using independent in vitro, Y2H, and bimolecular fluorescence complementation experiments and showed that PPD2 interacts with the C domain of NINJA, also known to interact with other members of the TIFY protein family (Vanholme et al., 2007; Pauwels et al., 2010; Bai et al., 2011; Zhang et al., 2012). In the future, however, it will be important to verify the PPD2-NINJA interaction in planta in a native context. In this study, we also showed that *ninja* loss-of-function mutants display propeller-like rosettes and a convex-shaped primary cell cycle arrest front that putatively leads to the formation of dome-shaped leaves. Because the expression of *PPD* genes is not affected upon JA treatment (Pauwels et al., 2010) and the phenotypes of *PPD* mutants are not related to JA signaling (White, 2006; Gonzalez et al., 2015), NINJA appears to play a pivotal role in limiting leaf curvature in addition to its function in mediating the JA-transcriptional response (Pauwels et al., 2010; Acosta et al., 2013; Gasperini et al., 2015), probably through its interaction with PPD2. A premature stop codon in *NINJA*, accompanied by a down-regulation in *NINJA* transcripts, prevents the PPD2-NINJA interaction and, therefore, the recruitment of TPL to the PPD2 repressor complex (Pauwels et al., 2010), causing the increased expression of downstream target genes of the protein complex (Fig. 8). The interaction between PPD and NINJA proteins was found not only in Arabidopsis (Pauwels et al., 2010) but also in *Medicago truncatula* (Ge et al., 2016; Goossens et al., 2016), suggesting that the PPD-NINJA complex might control the shape of the primary arrest front and, consequently, leaf flatness across eudicot plant species. This control of leaf shape likely occurs through the repression of *CYCD3* genes, but whether the PPD2-NINJA repressor complex binds directly or indirectly to the *CYCD3* loci is a subject for future research.

CYCD3 Family Members Have a Distinct Contribution to the Control of Leaf Flatness

The CYCD3 subfamily of D-type cyclins consists of three members: CYCD3;1, CYCD3;2, and CYCD3;3. CYCD3s are considered primarily to be redundant, and their roles have been studied mainly using the *cycd3;1 cycd3;2 cycd3;3* triple mutant (Dewitte et al., 2003, 2007). For some aspects of plant organ development, this redundancy is clearly demonstrated. For instance, only triple *cycd3* mutants lack a cytokinin response, being unable to produce shoots in response to high concentrations of this plant hormone (Dewitte et al., 2007). Nevertheless, the spatial and temporal expression patterns of the *CYCD3s* are only partially overlapping in both Arabidopsis (Dewitte et al., 2007) and tomato (*Solanum lycopersicum*; Kvarnheden et al., 2000). This implies that plant tissues might have different requirements for specific *CYCD3* expression and that CYCD3s might have very specific functions during plant development (Riou-Khamlichi et al., 1999, 2000; Kvarnheden et al., 2000; Dewitte et al., 2003, 2007), although this remains to be fully explored. The expression of *CYCD3;2* and *CYCD3;3* is enhanced in the *ami-ppd* mutants and the double *kix8 kix9* mutant, which has a decreased expression of two PPD2 interaction partners (Gonzalez et al., 2015), and, as shown here, in *ninja* mutants (Fig. 8). Despite the fact that *CYCD3;2* and *CYCD3;3* have a similar expression pattern in the leaf (Dewitte et al., 2007), ectopic expression of *CYCD3;2* but not of *CYCD3;3* resulted in propeller-like rosettes with dome-shaped leaves. Nevertheless, the dome-shaped leaf phenotype

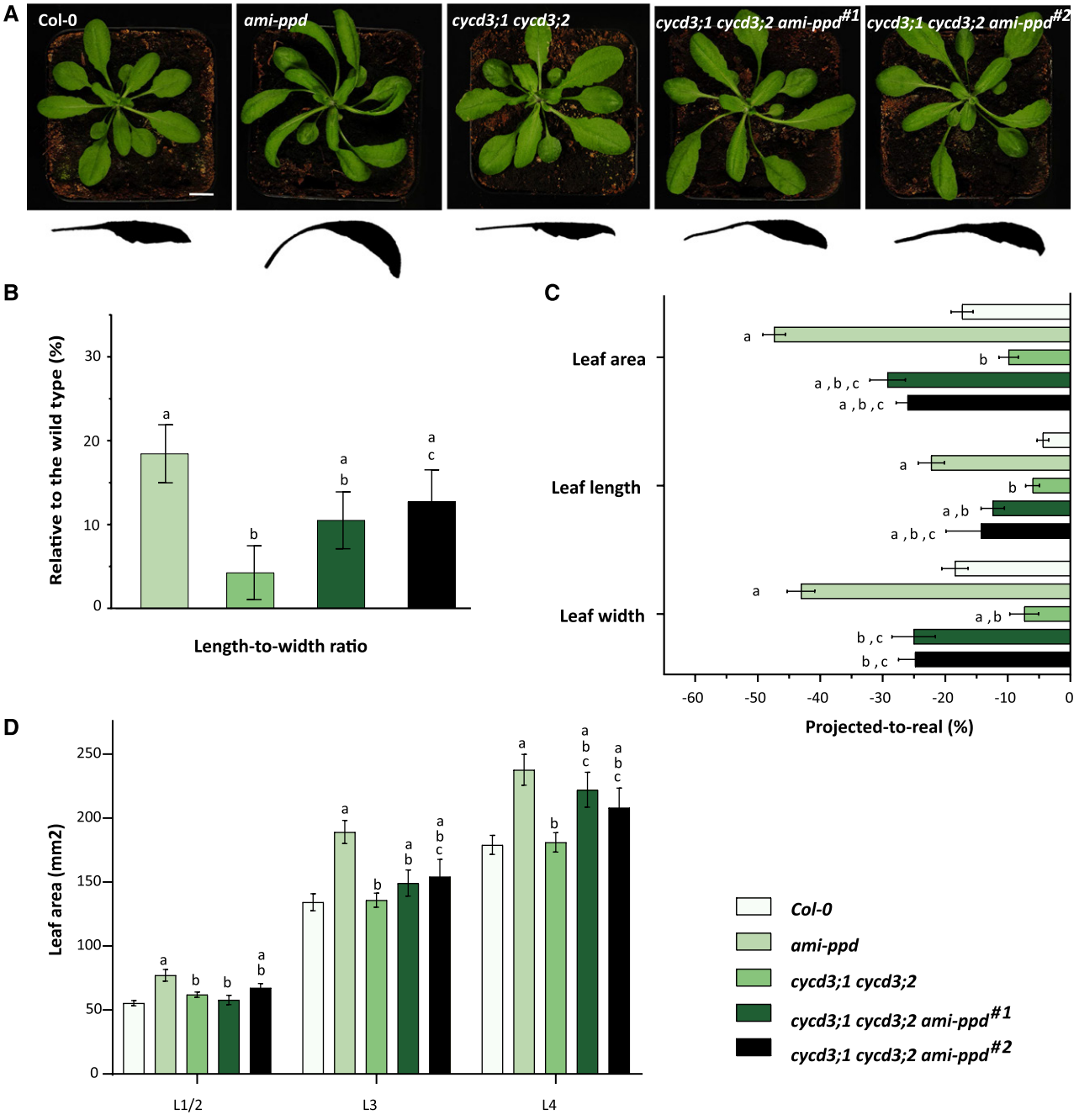

Figure 7. Inactivation of CYCD3;1 and CYCD3;2 decreases the extent of *ami-ppd* leaf curvature. A, Col-0, *ami-ppd*, *cycd3;1 cycd3;2*, *cycd3;1 cycd3;2 ami-ppd*$^{\#1}$, and *cycd3;1 cycd3;2 ami-ppd*$^{\#2}$ plants grown in soil for 25 d. Side views of the seventh leaf (L7) are presented below the photographs. Bar = 1 cm. B and C, Leaf 7 length-to-width ratio (B) and projected-to-real leaf area, length, and width (C) of Col-0, *ami-ppd*, *cycd3;1 cycd3;2*, *cycd3;1 cycd3;2 ami-ppd*$^{\#1}$, and *cycd3;1 cycd3;2 ami-ppd*$^{\#2}$ plants grown in soil for 25 d (n = 3 biological replicates with approximately eight plants per replicate). Error bars represent SE. Statistical significance was evaluated by ANOVA followed by Tukey's posthoc analysis. D, Area of leaves 1/2, 3, and 4 of Col-0, *ami-ppd*, *cycd3;1 cycd3;2*, *cycd3;1 cycd3;2 ami-ppd*$^{\#1}$, and *cycd3;1 cycd3;2 ami-ppd*$^{\#2}$ plants grown in soil for 25 d relative to Col-0 (n = 3 biological replicates with approximately eight plants per replicate), analyzed using mixed models in the SAS Enterprise Guide. In C and D, statistically significant differences ($P < 0.05$) relative to Col-0 (a), *ami-ppd* (b), *cycd3;1 cycd3;2* (c), and *cycd3;1 cycd3;2 ami-ppd*$^{\#1}$ (d) are indicated with lowercase letters.

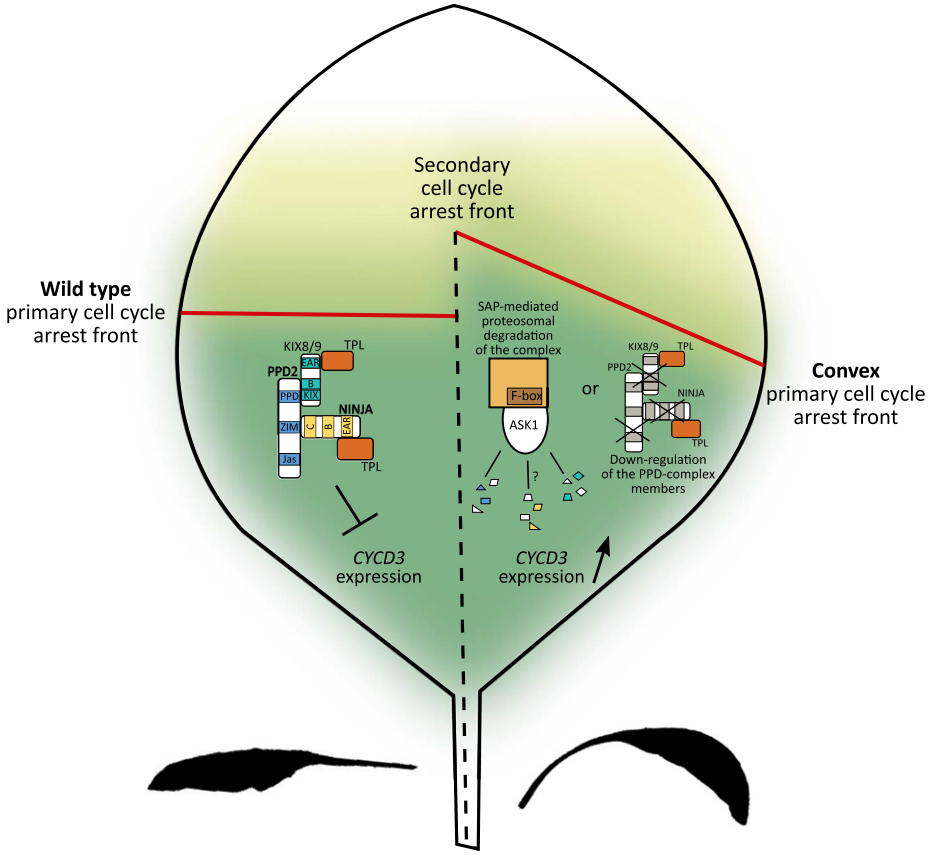

Figure 8. Schematic overview of the involvement of the PPD complex in leaf growth and shape control. In wild-type leaves, the PPD2 protein interacts with the adaptor proteins KIX8/9 and NINJA to recruit TPL, generating a transcriptional repressor complex. The complex inhibits the expression of downstream target genes, including *CYCD3s*, which results in a relatively straight primary cell cycle arrest front and a flat-leaf phenotype. Upon SAP-mediated proteosomal degradation or down-regulation of members of the repressor complex, the complex is inactive. This results in the overexpression of the *CYCD3* cell cycle genes, the formation of a convex primary cell cycle arrest front, and a dome-shaped leaf phenotype.

in *ppd* mutants could only be partially restored upon loss of function of *CYCD3;2* and *CYCD3;1*, although transcript levels of *CYCD3;1* were not changed in *ami-ppd* (Gonzalez et al., 2015) and *ninja* mutants at the selected time points. This indicates that there also might be a certain degree of redundancy among the CYCD3 proteins to control leaf shape. In the future, it will be interesting to uncover the individual contributions of the CYCD3 family members to the control of leaf flatness.

CYCD3;2 as a Central Node in the Control of the Cell Cycle, the Stomatal Lineage, and Leaf Shape

Arabidopsis leaves typically develop into flat structures to maximize the photosynthetic surface (Horiguchi et al., 2006; Rolland-Lagan et al., 2014). Because forming a flat structure requires uniform growth throughout the lamina, leaf flatness is strictly controlled by several regulatory pathways, including the PPD module (Nath et al., 2003; Palatnik et al., 2003; Horiguchi et al., 2006; Karidas et al., 2015). Based on the shape of the primary cell cycle arrest front in *ami-ppd* and *ninja* mutants and the increased expression of *CYCD3;2* in these mutants, we hypothesized that the curvature phenotype in *ppd* and *ninja* leaves is caused by the elevated expression of central to margin cyclins. Nonetheless, *CYCD3;2-OE* lines expressing *CYCD3;2* controlled by the cauliflower mosaic virus *35S* promoter displayed dome-shaped leaves. Constitutive overexpression of *CYCD3;2*, however, does not imply that CYCLIN-DEPENDENT KINASE (CDK) interaction partners, which are essential for the functionality of cyclins, are present. In addition, cyclins are highly prone to posttranslational regulations, further increasing the complexity by which cyclins might be regulated in individual cells. Previously, it has been shown that *CYCD3;2* expression is activated in meristemoids and declined gradually throughout the stomatal lineage, becoming undetectable in mature guard cells (Adrian et al., 2015). Correspondingly, *CYCD3;2* expression has been shown to be activated by SPEECHLESS (SPCH; Lau et al., 2014), a transcription factor that positively regulates meristemoid initiation and recurrent

asymmetric divisions (Bergmann and Sack, 2007; Lau and Bergmann, 2012; Pillitteri and Torii, 2012; Lau et al., 2014). The opposite regulation of *CYCD3;2* by PPD2 and SPCH and the gradual increase in guard cell number upon *CYCD3;2* overexpression suggest that a strict spatiotemporal control of *CYCD3;2* expression is not only essential to control leaf shape but also throughout the stomatal lineage. This is also concurrent with previous data showing that ectopic overexpression of *CYCLIN DEPENDENT KINASE A;1* (*CDKA;1*) and *CYCD3;2* from a *FAMA* promoter induces extra guard cell divisions, resulting in abnormal stomata with three to four guard cells (Yang et al., 2014). These data indicate that a timely dampening of CDKA;1-CYCD3 activity is essential to block guard cell division (Yang et al., 2014). CYCDs promote the progression of the cell cycle during the G1 phase and the G1-to-S transition (Menges et al., 2006; Magyar et al., 2012; Zhao et al., 2012). In complex with CDKs, they bind and phosphorylate RETINOBLASTOMA-RELATED (RBR), causing its degradation (Huntley et al., 1998; Nakagami et al., 1999). Interestingly, RBR has been shown previously to regulate the asymmetric divisions of meristemoids (Weimer et al., 2012), and plants with reduced *RBR* transcript levels also produce propeller-like rosettes with slightly dome-shaped leaves (Dorca-Fornell et al., 2013). All these findings indicate that a precise regulation of the pattern of cell cycle arrest is a key aspect in controlling leaf shape (Nath et al., 2003; Karidas et al., 2015) and underline the importance of a proper spatiotemporal regulation of *CYCD3* expression therein.

ninja and *CYCD3;2-OE* Plants Lack the Increased Leaf Size Observed in *ppd* Mutants

In this study, we demonstrated that, even though *ninja* and *CYCD3;2-OE* plants show the *ppd* dome-shaped leaf phenotype and increased guard and pavement cell numbers, they do not produce larger leaves. The PPD proteins have been suggested to act on both the primary (Karidas et al., 2015) and secondary (White, 2006; Gonzalez et al., 2015) mitotic arrest fronts in leaves, referring to the division of pavement and meristemoid cells, respectively. Consequently, the increased leaf area observed in *ppd* mutants results, at least partially, from a drastic increase in meristemoid asymmetric divisions (White, 2006; Gonzalez et al., 2015). Interestingly, however, meristemoid asymmetric divisions were not increased in the abaxial epidermis of *CYCD3;2-OE* plants. This suggests that the increase in pavement cell number and the decrease in stomatal index in *CYCD3;2-OE* leaves result solely from an altered primary cell cycle arrest phase. The dissimilarity between *ppd* and *CYCD3;2-OE* plants regarding meristemoid asymmetric divisions and leaf size implies that the role of PPD2 in leaf size and shape control could be partially uncoupled and, to a certain extent, might be regulated differently. Consequently, the leaf shape and size phenotype in *ppd* mutants could be the cumulative output of distinct downstream regulatory pathways. In addition to the dome-shaped leaf phenotype, PPD signaling mutants produce rosettes with a propeller-like appearance. However, we hypothesize that the rosette phenotype is not necessarily related to the dome-shaped leaf phenotype but might be caused by alterations in vasculature development, a process in which PPDs have been proposed to be involved (White, 2006). The contribution of the PPD module to vasculature development could be governed by *CYCD3* genes and/or by other unidentified target genes of the complex. Mediating the expression of additional downstream target genes besides *CYCD3s* might be a way to control distinct pathways to regulate a variety of growth and developmental processes.

The PPD Module Controls Leaf Flatness and Is Highly Conserved in Eudicots

Several studies in different plant species have consistently shown the importance of the PPD signaling pathway in organ size and shape control, including seeds, seed pods, and leaves (Gonzalez et al., 2015; Ge et al., 2016; Wang et al., 2016; Naito et al., 2017; Yordanov et al., 2017; Kanazashi et al., 2018). The *mtbs1-1* mutant harbors a point mutation in *BIG SEEDS1* (*BS1*), encoding a putative PPD ortholog in *M. truncatula* (Ge et al., 2016). The *mtbs1-1* mutant and *VmPPD* mutant in *Vigna mungo* (Naito et al., 2017) produce enlarged seeds and leaves with similarities to those of Arabidopsis *ppd* mutants (White, 2006; Gonzalez et al., 2015). Down-regulation of the putative *PPD* orthologs in soybean (*Glycine max*) using an artificial microRNA significantly increased soybean seed size, weight, and amino acid content (Ge et al., 2016; Naito et al., 2017). More recently, *GmPPD1* and *GmPPD2* double mutants have been generated in soybean using the CRISPR/Cas9 technology; they also displayed dome-shaped trifoliate leaves and twisted pods containing fewer but enlarged seeds compared with wild-type plants (Kanazashi et al., 2018). The PPD complex is degraded in a proteasome-dependent manner by the Arabidopsis SCF complex containing the F-box protein STERILE APETALA (SAP; Fig. 8; Wang et al., 2016; Li et al., 2018). Overexpression of *SAP* in Arabidopsis (Wang et al., 2016) and of the poplar *SAP* ortholog *BIG LEAF* (Yordanov et al., 2017) resulted in plants with enlarged leaves and uneven lamina growth. Despite the common importance of the PPD2/KIX8/KIX9/SAP complex for organ size and shape determination in eudicots, it is lost in Poaceae (grasses; Gonzalez et al., 2015; Nelissen et al., 2016; Wang et al., 2016). In agreement, self-renewing meristemoid-like cells and a secondary cell cycle arrest front moving through the leaf blade, in which PPD2 is involved, are fundamental for eudicot leaf development but absent in grasses (Liu et al., 2009). By contrast, NINJA is present in all land plants and is essential in JA signaling (Sheard et al., 2010; Thaler et al., 2012) as well as in controlling leaf flatness through regulation of the shape of the primary cell cycle arrest front. The observation that NINJA

orthologs are present in grasses such as maize (*Zea mays*) and rice (*Oryza sativa*) further strengthens their broader role in plant development.

MATERIALS AND METHODS

In Vitro Pull-Down Assay

The coding sequence of *PPD2* was inserted into the *Bam*HI and *Eco*RI sites of the *pGEX-4T-1* vector to obtain the *GST-PPD2* construct. The coding sequence of *NINJA* was inserted into the *Eco*RI and *Sal*I sites of the *pET-28a* (+) vector to construct the *His-NINJA* plasmid. The primer sequences are listed in Supplemental Table S1. To test the interaction of NINJA with PPD2, bacterial lysates containing ~30 µg of GST-PPD2 fusion proteins were combined with lysates containing ~30 µg of His-NINJA fusion proteins. A total of 20 µL of glutathione-Sepharose (GE Healthcare) was added into each combination and shaken gently at 4°C for 1 h. TGH buffer (50 mM HEPES, pH 7.5, 1.5 mM $MgCl_2$, 150 mM NaCl, 1 mM EGTA, 10% [v/v] glycerol, 1% [v/v] Triton X-100, 1 mM PMSF, and 1× Complete protease inhibitor cocktail) was used to wash the beads. The isolated proteins were separated further by SDS-PAGE and examined by immunoblot analysis using anti-GST (Abmart; 1:5,000) and anti-His (Abmart; 1:2,000) antibodies. Signals were detected using the eECL Western Blot Kit (CWBiotech; CW0049), and images were scanned using Tanon-4500 according to the manufacturer's instructions.

Bimolecular Fluorescence Complementation Assay

nYFP was amplified from the plasmid *pSY736*, fused to *NINJA*, and inserted into the *pDONR221* vector (Invitrogen). *cYFP* was amplified from the plasmid *pSY735*, fused to *PPD2*, and inserted into the *pDONR221* vector (Invitrogen). The primer sequences are listed in Supplemental Table S1. *nYFP-NINJA* and *cYFP-PPD2* constructs were cloned into the Gateway binary vector *pGWB414* by LR reactions (Invitrogen) and transformed into *Agrobacterium tumefaciens* (strain C58C1, pMP90). *A. tumefaciens* strains containing *nYFP-NINJA*, *cYFP-PPD2*, and *cYFP* plasmids were resuspended in buffer (10 mM MES, pH 5.6, 150 µM acetosyringone, and 10 mM $MgCl_2$), mixed, and coinfiltrated into *Nicotiana benthamiana* leaves. After infiltration, plants were grown for 2 d and fluorescence was detected using confocal microscopy (Zeiss LSM 710).

Y2H Experiments

A deletion series of *NINJA* and *PPD2* were cloned without stop codon into Gateway-compatible entry clones. The entry vectors were used for LR reactions (Invitrogen) with *pGADT7* and *pGBKT7* (or *pGBT9*) Y2H vectors, generating bait and prey constructs. Cotransformation of the *Saccharomyces cerevisiae* PJ69-4A yeast strain using different bait-prey plasmid combinations was performed according to Cuéllar Pérez et al. (2014). Transformed yeast colonies were selected on SD medium lacking Leu and Trp. To verify a possible interaction, several independent yeast colonies were grown on selective medium lacking Leu, Trp, and His for 3 to 4 d at 30°C. Cotransformation with the empty *pGADT7* and *pGBKT7* (or *pGBT9*) vectors was used as a negative control.

Plant Material and Growth Conditions

The Arabidopsis (*Arabidopsis thaliana*) *ami-ppd* line is described by Gonzalez et al. (2015). The *cycd3;2* mutant (GK396C10) was obtained from the GABI-KAT T-DNA collection (Sessions et al., 2002) and genotyped by PCR to verify homozygosity. The *ninja-1*, *ninja-2*, *ninja-1 aos*, *ninja-2 aos*, and *ninja-1 coi1-1* lines were kindly provided by Debora Gasperini (Leibniz Institute of Plant Biochemistry). *ninja-1* and *ninja-2* were described by Acosta et al. (2013) and have a mutation in Chr4:14265008 (C to T) and Chr4:14264791 (G to A), respectively, resulting in a stop codon Q225* in *ninja-1* and an affected first intron/exon split in *ninja-2*. The *cycd3;1 cycd3;2* double mutant line was kindly provided by Walter Dewitte and Jim Murray (Cardiff University). The coding sequences of *CYCD3;2* and *CYCD3;3* were PCR amplified from Col-0 cDNA and introduced into *pDONR221*. The *35S::CYCD3;2* and *35S::CYCD3;3* constructs were cloned by Multisite Gateway cloning (Invitrogen) into *pK7m24GW;3_FAST* and *pFAST-G02*, respectively (Karimi et al., 2002). The expression vectors were used for the transformation of Arabidopsis Col-0 plants with the floral dip method using *A. tumefaciens* (strain C58C1, pMP90; Clough and Bent, 1998). Transformants were selected on medium supplied with the corresponding antibiotic, and homozygous single-locus insertion plants were used in the experiments. For the genetic interaction studies, *ami-ppd* and *cycd3;1 cycd3;2 ami-ppd* transgenic lines with a single-locus insertion and with a similar down-regulation of *PPD2* transcripts were obtained and selected for further analysis (Supplemental Fig. S6). Experiments were performed with segregating wild-type and transgenic seeds harvested from plants that were grown in parallel. For molecular experiments, plants were surface sterilized and grown in vitro for 14 d on solid (9 g L^{-1} agar; Sigma) one-half-strength Murashige and Skoog medium (Murashige and Skoog, 1962) supplemented with 1% (w/v) Suc. For phenotyping experiments, plants were grown in soil for 21 or 25 d. In vitro and in soil, plants were stratified for 3 d at 4°C and grown at 21°C under a 16-h-day/8-h-night regime.

Histochemical GUS Analysis

Histochemical GUS staining was performed on young developing leaves of *pCYCB1;1-DB::GUS* (leaf 10), *ami-ppd pCYCB1;1-DB::GUS* (leaf 10), and *ninja-2 pCYCB1;1-DB::GUS* (leaf 9) plants grown in soil for 21 d. The plant material was incubated in the dark in a staining buffer containing 1 mM 5-bromo-4-chloro-3-indolyl β-D-glucopyranoside sodium salt, 0.5% (v/v) Triton X-100, 1 mM EDTA, pH 8, 0.5 mM potassium ferricyanide [$K_3Fe(CN)_6$], 0.5 mM potassium ferricyanide [$K_4Fe(CN)_6$], and 500 mM sodium phosphate buffer, pH 7. After an overnight incubation at 37°C, leaves were decolored by replacing the staining buffer with 100% ethanol. The material was mounted in lactic acid and analyzed with a binocular microscope (Leica; MZ16). The experiment was performed in three biological replicates with ~20 leaves each.

RNA Isolation and qRT-PCR Analysis

Total RNA was isolated from the first leaf pair (L1/2) of 14-d-old plants with Trizol (Invitrogen), purified with the RNeasy Plant Mini Kit (Qiagen), and treated with DNase I (Promega). cDNA was obtained with the iScript cDNA Synthesis Kit (Bio-Rad) according to the manufacturer's instructions. Relative transcript abundance was determined using the Roche LightCycler 480 and the LC480 SYBR Green I Master Kit (Roche Diagnostics). The resulting cycle threshold values were converted into relative expression values using the second derivative maximum method. *CDKA* and *CBP20* were used as reference genes for normalization. All experiments were performed in three biological replicates (approximately five leaves per replicate), each with three technical replicates. The primer sequences are listed in Supplemental Table S1.

Leaf Growth Parameters

Plants were grown in soil for 25 d. For the leaf series analysis, individual leaf areas were measured with the ImageJ software (https://imagej.nih.gov/ij/). For the leaf shape analysis, the seventh leaf (L7) was harvested and photographs were taken before and after cutting the leaves to flatten them. Projected and real leaf area, length, and width and the leaf perimeter were measured using ImageJ. For the cellular analysis, the leaves were cleared with 100% ethanol, mounted in lactic acid on microscope slides, and abaxial epidermal cells (~300 cells) were drawn for three biological replicates (four leaves each) with a binocular microscope (Leica; DMLB) fitted with a drawing tube and a differential interference contrast objective. Average guard, pavement, and total cell numbers, as well as pavement cell area and stomatal index, were calculated as described previously (Andriankaja et al., 2012). Leaf imprints were made daily from the abaxial surface of the first leaf pair (L1/2) from day 12 to day 14 according to Kagan et al. (1992). Nail polish impressions were made and analyzed by scanning electron microscopy (Hitachi; TM-1000 Tabletop Microscope). The fate of meristemoid cells was analyzed over time by evaluating whether a meristemoid became a guard mother cell or a stoma and whether it divided asymmetrically or remained unchanged.

Statistical Tests

For the leaf series analysis, statistical tests were performed with the mixed models and plm procedure in the SAS Enterprise Guide as described previously (Blomme et al., 2014). In the presence of a significant F test ($P < 0.05$), pairwise comparisons among the transgenic lines or between the transgenic lines and the segregating wild type were performed using Tukey's posthoc test. For

each leaf, correction for multiple testing was done according to Dunnett. For the statistical analysis of the leaf curvature and for the cellular and expression data, ANOVA was performed in R (version 3.3.2; https://www.r-project.org) using Tukey's posthoc analysis ($P < 0.05$). For all statistical tests, the transgenic line was the fixed factor in the model. Biological replicates were included as a random factor.

Accession Numbers

Accession numbers are as follows: AT4G14720 (PPD2), AT4G28910 (NINJA), AT4G34160 (CYCD3;1), AT5G67260 (CYCD3;2), AT3G50070 (CYCD3;3), AT3G24150 (KIX8), and AT4G32295 (KIX9).

Supplemental Data

The following supplemental materials are available.

Supplemental Figure S1. The expression of *NINJA* is decreased in *ninja* mutants.

Supplemental Figure S2. The *ninja* leaf phenotype is not affected by a decreased JA response.

Supplemental Figure S3. Leaf length, width, and perimeter in PPD2 signaling mutants.

Supplemental Figure S4. Inactivation of CYCD3;2 does not complement the *ppd2* leaf phenotype.

Supplemental Figure S5. The expression of *CYCD3;1* is not changed in *ninja* mutants.

Supplemental Figure S6. Residual *PPD2* expression in the *ami-ppd* and *cycd3;1 cycd3;2 ami-ppd* mutants.

Supplemental Table S1. Primers used in this study.

ACKNOWLEDGMENTS

We thank Carina Braeckman and Mieke Van Lijsebettens for assistance in generating the Arabidopsis transgenic lines, Karel Spruyt for imaging assistance, and Annick Bleys for the help in preparing the article. We also thank Debora Gasperini (*ninja-1*, *ninja-2*, *aos*, *ninja-1 coi1-1*, *ninja-1 aos*, and *ninja-2 aos*), Walter Dewitte, and Jim Murray (*cycd3;1 cycd3;2*) for kindly providing some of the transgenic lines used in this study.

Received March 19, 2018; accepted June 28, 2018; published July 10, 2018.

LITERATURE CITED

Acosta IF, Gasperini D, Chételat A, Stolz S, Santuari L, Farmer EE (2013) Role of NINJA in root jasmonate signaling. Proc Natl Acad Sci USA **110**: 15473–15478

Adrian J, Chang J, Ballenger CE, Bargmann BOR, Alassimone J, Davies KA, Lau OS, Matos JL, Hachez C, Lanctot A, (2015) Transcriptome dynamics of the stomatal lineage: birth, amplification, and termination of a self-renewing population. Dev Cell **33**: 107–118

Andriankaja M, Dhondt S, De Bodt S, Vanhaeren H, Coppens F, De Milde L, Mühlenbock P, Skirycz A, Gonzalez N, Beemster GTS, (2012) Exit from proliferation during leaf development in *Arabidopsis thaliana*: a not-so-gradual process. Dev Cell **22**: 64–78

Bai Y, Meng Y, Huang D, Qi Y, Chen M (2011) Origin and evolutionary analysis of the plant-specific TIFY transcription factor family. Genomics **98**: 128–136

Bergmann DC, Sack FD (2007) Stomatal development. Annu Rev Plant Biol **58**: 163–181

Bilsborough GD, Runions A, Barkoulas M, Jenkins HW, Hasson A, Galinha C, Laufs P, Hay A, Prusinkiewicz P, Tsiantis M (2011) Model for the regulation of *Arabidopsis thaliana* leaf margin development. Proc Natl Acad Sci USA **108**: 3424–3429

Blomme J, Inzé D, Gonzalez N (2014) The cell-cycle interactome: a source of growth regulators? J Exp Bot **65**: 2715–2730

Clough SJ, Bent AF (1998) Floral dip: a simplified method for *Agrobacterium*-mediated transformation of *Arabidopsis thaliana*. Plant J **16**: 735–743

Cuéllar Pérez A, Nagels Durand A, Vanden Bossche R, De Clercq R, Persiau G, Van Wees SCM, Pieterse CMJ, Gevaert K, De Jaeger G, Goossens A, (2014) The non-JAZ TIFY protein TIFY8 from *Arabidopsis thaliana* is a transcriptional repressor. PLoS ONE **9**: e84891

Dewitte W, Riou-Khamlichi C, Scofield S, Healy JMS, Jacqmard A, Kilby NJ, Murray JAH (2003) Altered cell cycle distribution, hyperplasia, and inhibited differentiation in *Arabidopsis* caused by the D-type cyclin CYCD3. Plant Cell **15**: 79–92

Dewitte W, Scofield S, Alcasabas AA, Maughan SC, Menges M, Braun N, Collins C, Nieuwland J, Prinsen E, Sundaresan V, (2007) *Arabidopsis* CYCD3 D-type cyclins link cell proliferation and endocycles and are rate-limiting for cytokinin responses. Proc Natl Acad Sci USA **104**: 14537–14542

Dkhar J, Pareek A (2014) What determines a leaf's shape? Evodevo **5**: 47

Donnelly PM, Bonetta D, Tsukaya H, Dengler RE, Dengler NG (1999) Cell cycling and cell enlargement in developing leaves of *Arabidopsis*. Dev Biol **215**: 407–419

Dorca-Fornell C, Pajor R, Lehmeier C, Pérez-Bueno M, Bauch M, Sloan J, Osborne C, Rolfe S, Sturrock C, Mooney S, (2013) Increased leaf mesophyll porosity following transient retinoblastoma-related protein silencing is revealed by microcomputed tomography imaging and leads to a system-level physiological response to the altered cell division pattern. Plant J **76**: 914–929

Efroni I, Blum E, Goldshmidt A, Eshed Y (2008) A protracted and dynamic maturation schedule underlies *Arabidopsis* leaf development. Plant Cell **20**: 2293–2306

Elsner J, Michalski M, Kwiatkowska D (2012) Spatiotemporal variation of leaf epidermal cell growth: a quantitative analysis of *Arabidopsis thaliana* wild-type and triple *cyclinD3* mutant plants. Ann Bot **109**: 897–910

Feys B, Benedetti CE, Penfold CN, Turner JG (1994) *Arabidopsis* mutants selected for resistance to the phytotoxin coronatine are male sterile, insensitive to methyl jasmonate, and resistant to a bacterial pathogen. Plant Cell **6**: 751–759

Gasperini D, Chételat A, Acosta IF, Goossens J, Pauwels L, Goossens A, Dreos R, Alfonso E, Farmer EE (2015) Multilayered organization of jasmonate signalling in the regulation of root growth. PLoS Genet **11**: e1005300

Ge L, Yu J, Wang H, Luth D, Bai G, Wang K, Chen R (2016) Increasing seed size and quality by manipulating *BIG SEEDS1* in legume species. Proc Natl Acad Sci USA **113**: 12414–12419

Geisler M, Nadeau J, Sack FD (2000) Oriented asymmetric divisions that generate the stomatal spacing pattern in *Arabidopsis* are disrupted by the *too many mouths* mutation. Plant Cell **12**: 2075–2086

Gonzalez N, Pauwels L, Baekelandt A, De Milde L, Van Leene J, Besbrugge N, Heyndrickx KS, Cuéllar Pérez A, Durand AN, De Clercq R, (2015) A repressor protein complex regulates leaf growth in *Arabidopsis*. Plant Cell **27**: 2273–2287

Goossens J, De Geyter N, Walton A, Eeckhout D, Mertens J, Pollier J, Fiallos-Jurado J, De Keyser A, De Clercq R, Van Leene J, (2016) Isolation of protein complexes from the model legume *Medicago truncatula* by tandem affinity purification in hairy root cultures. Plant J **88**: 476–489

Horiguchi G, Ferjani A, Fujikura U, Tsukaya H (2006) Coordination of cell proliferation and cell expansion in the control of leaf size in *Arabidopsis thaliana*. J Plant Res **119**: 37–42

Huntley R, Healy S, Freeman D, Lavender P, de Jager S, Greenwood J, Makker J, Walker E, Jackman M, Xie Q, (1998) The maize retinoblastoma protein homologue ZmRb-1 is regulated during leaf development and displays conserved interactions with G1/S regulators and plant cyclin D (CycD) proteins. Plant Mol Biol **37**: 155–169

Kagan ML, Novoplansky N, Sachs T (1992) Variable cell lineages form the functional pea epidermis. Ann Bot **69**: 303–312

Kanazashi Y, Hirose A, Takahashi I, Mikami M, Endo M, Hirose S, Toki S, Kaga A, Naito K, Ishimoto M, (2018) Simultaneous site-directed mutagenesis of duplicated loci in soybean using a single guide RNA. Plant Cell Rep **37**: 553–563

Karidas P, Challa KR, Nath U (2015) The *tarani* mutation alters surface curvature in *Arabidopsis* leaves by perturbing the patterns of surface expansion and cell division. J Exp Bot **66**: 2107–2122

Karimi M, Inzé D, Depicker A (2002) GATEWAY vectors for *Agrobacterium*-mediated plant transformation. Trends Plant Sci **7**: 193–195

Kazama T, Ichihashi Y, Murata S, Tsukaya H (2010) The mechanism of cell cycle arrest front progression explained by a *KLUH/CYP78A5*-dependent mobile growth factor in developing leaves of *Arabidopsis thaliana*. Plant Cell Physiol **51**: 1046–1054

Kvarnheden A, Yao JL, Zhan X, O'Brien I, Morris BAM (2000) Isolation of three distinct *CycD3* genes expressed during fruit development in tomato. J Exp Bot **51**: 1789–1797

Lau OS, Bergmann DC (2012) Stomatal development: a plant's perspective on cell polarity, cell fate transitions and intercellular communication. Development **139**: 3683–3692

Lau OS, Davies KA, Chang J, Adrian J, Rowe MH, Ballenger CE, Bergmann DC (2014) Direct roles of SPEECHLESS in the specification of stomatal self-renewing cells. Science **345**: 1605–1609

Li N, Liu Z, Wang Z, Ru L, Gonzalez N, Baekelandt A, Pauwels L, Goossens A, Xu R, Zhu Z, (2018) STERILE APETALA modulates the stability of a repressor protein complex to control organ size in *Arabidopsis thaliana*. PLoS Genet **14**: e1007218

Li R, Wang M, Wang Y, Schuman MC, Weinhold A, Schäfer M, Jiménez-Alemán GH, Barthel A, Baldwin IT (2017) Flower-specific jasmonate signaling regulates constitutive floral defenses in wild tobacco. Proc Natl Acad Sci USA **114**: E7205–E7214

Liu T, Ohashi-Ito K, Bergmann DC (2009) Orthologs of *Arabidopsis thaliana* stomatal bHLH genes and regulation of stomatal development in grasses. Development **136**: 2265–2276

Magyar Z, Horváth B, Khan S, Mohammed B, Henriques R, De Veylder L, Bakó L, Scheres B, Bögre L (2012) *Arabidopsis* E2FA stimulates proliferation and endocycle separately through RBR-bound and RBR-free complexes. EMBO J **31**: 1480–1493

Menges M, Samland AK, Planchais S, Murray JA (2006) The D-type cyclin CYCD3;1 is limiting for the G1-to-S-phase transition in *Arabidopsis*. Plant Cell **18**: 893–906

Murashige T, Skoog F (1962) A revised medium for rapid growth and bio assays with tobacco tissue cultures. Physiol Plant **15**: 473–497

Naito K, Takahashi Y, Chaitieng B, Hirano K, Kaga A, Takagi K, Ogiso-Tanaka E, Thavarasook C, Ishimoto M, Tomooka N (2017) Multiple organ gigantism caused by mutation in *VmPPD* gene in blackgram (*Vigna mungo*). Breed Sci **67**: 151–158

Nakagami H, Sekine M, Murakami H, Shinmyo A (1999) Tobacco retinoblastoma-related protein phosphorylated by a distinct cyclin-dependent kinase complex with Cdc2/cyclin D *in vitro*. Plant J **18**: 243–252

Nath U, Crawford BCW, Carpenter R, Coen E (2003) Genetic control of surface curvature. Science **299**: 1404–1407

Nelissen H, Gonzalez N, Inzé D (2016) Leaf growth in dicots and monocots: so different yet so alike. Curr Opin Plant Biol **33**: 72–76

Palatnik JF, Allen E, Wu X, Schommer C, Schwab R, Carrington JC, Weigel D (2003) Control of leaf morphogenesis by microRNAs. Nature **425**: 257–263

Park JH, Halitschke R, Kim HB, Baldwin IT, Feldmann KA, Feyereisen R (2002) A knock-out mutation in allene oxide synthase results in male sterility and defective wound signal transduction in *Arabidopsis* due to a block in jasmonic acid biosynthesis. Plant J **31**: 1–12

Pauwels L, Barbero GF, Geerinck J, Tilleman S, Grunewald W, Pérez AC, Chico JM, Bossche RV, Sewell J, Gil E, (2010) NINJA connects the co-repressor TOPLESS to jasmonate signalling. Nature **464**: 788–791

Pérez-Pérez JM, Serrano-Cartagena J, Micol JL (2002) Genetic analysis of natural variations in the architecture of *Arabidopsis thaliana* vegetative leaves. Genetics **162**: 893–915

Pillitteri LJ, Torii KU (2012) Mechanisms of stomatal development. Annu Rev Plant Biol **63**: 591–614

Riou-Khamlichi C, Huntley R, Jacqmard A, Murray JAH (1999) Cytokinin activation of *Arabidopsis* cell division through a D-type cyclin. Science **283**: 1541–1544

Riou-Khamlichi C, Menges M, Healy JMS, Murray JAH (2000) Sugar control of the plant cell cycle: differential regulation of *Arabidopsis* D-type cyclin gene expression. Mol Cell Biol **20**: 4513–4521

Rolland-Lagan AG, Remmler L, Girard-Bock C (2014) Quantifying shape changes and tissue deformation in leaf development. Plant Physiol **165**: 496–505

Sessions A, Burke E, Presting G, Aux G, McElver J, Patton D, Dietrich B, Ho P, Bacwaden J, Ko C, (2002) A high-throughput *Arabidopsis* reverse genetics system. Plant Cell **14**: 2985–2994

Sheard LB, Tan X, Mao H, Withers J, Ben-Nissan G, Hinds TR, Kobayashi Y, Hsu FF, Sharon M, Browse J, (2010) Jasmonate perception by inositol-phosphate-potentiated COI1-JAZ co-receptor. Nature **468**: 400–405

Thaler JS, Humphrey PT, Whiteman NK (2012) Evolution of jasmonate and salicylate signal crosstalk. Trends Plant Sci **17**: 260–270

Thines B, Katsir L, Melotto M, Niu Y, Mandaokar A, Liu G, Nomura K, He SY, Howe GA, Browse J (2007) JAZ repressor proteins are targets of the SCFCOI1 complex during jasmonate signalling. Nature **448**: 661–665

Vanholme B, Grunewald W, Bateman A, Kohchi T, Gheysen G (2007) The tify family previously known as ZIM. Trends Plant Sci **12**: 239–244

Vlad D, Kierzkowski D, Rast MI, Vuolo F, Dello Ioio R, Galinha C, Gan X, Hajheidari M, Hay A, Smith RS, (2014) Leaf shape evolution through duplication, regulatory diversification, and loss of a homeobox gene. Science **343**: 780–783

Wang L, Wu SM, Zhu Y, Fan Q, Zhang ZN, Hu G, Peng QZ, Wu JH (2017) Functional characterization of a novel jasmonate ZIM-domain interactor (NINJA) from upland cotton (*Gossypium hirsutum*). Plant Physiol Biochem **112**: 152–160

Wang Z, Li N, Jiang S, Gonzalez N, Huang X, Wang Y, Inzé D, Li Y (2016) SCFSAP controls organ size by targeting PPD proteins for degradation in *Arabidopsis thaliana*. Nat Commun **7**: 11192

Weimer AK, Nowack MK, Bouyer D, Zhao X, Harashima H, Naseer S, De Winter F, Dissmeyer N, Geldner N, Schnittger A (2012) Retinoblastoma related1 regulates asymmetric cell divisions in *Arabidopsis*. Plant Cell **24**: 4083–4095

White DWR (2006) *PEAPOD* regulates lamina size and curvature in *Arabidopsis*. Proc Natl Acad Sci USA **103**: 13238–13243

Yang K, Wang H, Xue S, Qu X, Zou J, Le J (2014) Requirement for A-type cyclin-dependent kinase and cyclins for the terminal division in the stomatal lineage of *Arabidopsis*. J Exp Bot **65**: 2449–2461

Yordanov YS, Ma C, Yordanova E, Meilan R, Strauss SH, Busov VB (2017) *BIG LEAF* is a regulator of organ size and adventitious root formation in poplar. PLoS ONE **12**: e0180527

Zhang Y, Gao M, Singer SD, Fei Z, Wang H, Wang X (2012) Genome-wide identification and analysis of the *TIFY* gene family in grape. PLoS ONE **7**: e44465

Zhao X, Harashima H, Dissmeyer N, Pusch S, Weimer AK, Bramsiepe J, Bouyer D, Rademacher S, Nowack MK, Novak B, (2012) A general G1/S-phase cell-cycle control module in the flowering plant *Arabidopsis thaliana*. PLoS Genet **8**: e1002847